PLANE-BASED CAMERA CALIBRATION WITHOUT DIRECT OPTIMIZATION ALGORITHMS

Jorge A. Sánchez, Eduardo A. Destefanis, Luis R. Canali

Centro de Investigación en Informática para Ingeniería,
Univ. Tecnológica Nacional, Facultad Regional Córdoba, Argentina.
edestefanis@scdt.utn.frc.edu.ar

Abstract: A new procedure for the calibration of a camera through the observation of a flat pattern from different points of view is proposed. Effects of lens distortion on the estimation of a homography between the model plane and its image have been considered, obtaining a simultaneous estimate of this homography and the distortion coefficients. As the distortion is mainly radial, it is necessary to estimate previously the coordinates of the principal point so that they can be used for estimation of the distortion coefficients. The comparison of this method with current non-linear optimization methods is shown in the paper.

Keywords Computer vision, camera calibration, lens distortion, camera model, photogrammetry.

1. INTRODUCTION

By "camera calibration" we understand the extraction of the set of parameters relating the space under observation to the image obtained in such space. A variety of methods have been developed for this purpose which could be generally classified into:

a. *Linear methods* comprising the solution of a linear system of equations, which implies an advantage as regards speed and simplicity; however, the accuracy achieved with them is very poor and, besides, they do not include the effects of the distortion produced by the lens system (Abdel-Aziz and Karara, 1971; Tsai, 1987; Knight, *et al.*, 2003).
b. *Non-linear methods* comprising non-linear optimization methods by means of which much better results are obtained since they allow for the inclusion of (non-linear) distortion parameters. Their inherent disadvantage is the high computational demand required. These methods comprise a solution in a closed manner which may serve as an initial estimate of the final optimization algorithm (Heikkil and Silvn, 1997; Hartley, 1994).

The accuracy obtained depends largely on the parameter set adopted to model the camera and its lens system. The most widespread model, especially in computer applications aimed at obtaining 3D measures (Fusiello, *et al.*, 2000; Farbiz, *et al.*, 2005), is the "pinhole" model.

The latter can be defined as a transformation between the coordinate system of the 3D space under observation and the camera coordinate system (extrinsic parameters), and then the transformation of a mapping of the points of said space to 2D points on the image plane (intrinsic parameters). This model is insufficient most of the times due to the presence of inherent distortions caused by the lens systems, which make the image to deflect considerably from the linear model in many cases. One way to overcome this disadvantage is the inclusion of distortion parameters in the model, which, added to the former parameters, become necessary information in applications which require the extraction of metric data from the space under observation.

This work is organized as follows: in the first part, the model of a pinhole camera and the manner of representing the most significant distortions are described. In the second part, the process of parameter estimation and the solution in the closed manner is adopted. Finally, in the third part, the comparative results with the method proposed by Zhang are shown.

2. CAMERA MODEL

By adopting the pinhole model and following the notation used in the Zhang's referenced paper, we can relate one point in the 3D space to the 2D point projected on the image, both in homogenous coordinates, by means of the following transformation:

$$s\begin{bmatrix} u \\ v \\ 1 \end{bmatrix} = \mathbf{A}\cdot[\mathbf{R}\,|\,\mathbf{t}]\cdot\begin{bmatrix} x_w \\ y_w \\ z_w \\ 1 \end{bmatrix} = \mathbf{A}\cdot\begin{bmatrix} x \\ y \\ z \\ 1 \end{bmatrix} \tag{1}$$

where s is an arbitrary scale factor, $[u, v, 1]^T$ are the coordinates of the 2D point projected on the image, $[x_w, y_w, z_w, 1]^T$ are the coordinates of the point in the reference frame of the 3D space, and $[x, y, z, 1]^T$ are the coordinates of the same 3D point, but respect to the coordinate system of the camera. **R** represents the rotation of the coordinate system of the 3D points with respect to the origin $(x_{w0}, y_{w0}, z_{w0}, 1)$, **t** is a vector representing the translation of the origin of the coordinate system of the 3D space to the origin of the camera coordinate system, $(x_0, y_0, z_0, 1)$, and **A** is a 3x3 matrix given by

$$\mathbf{A} = \begin{bmatrix} \alpha & c & u_0 \\ 0 & \beta & v_0 \\ 0 & 0 & 1 \end{bmatrix} \tag{2}$$

where (u_0, v_0) represent the coordinates of the principal point, c is a factor reflecting the skewness of the image axes, and α and β represent, respectively, the scale factors on the u and v axes of said image. In the set of parameters described, **R** and **t** correspond to the extrinsic parameters, while **A** corresponds to the intrinsic parameters.

Based on the pinhole model, and considering the case in which the points of interest are on the same plane, we can choose the reference system so that said plane is on $z_w=0$, which leads to:

$$s\begin{bmatrix} u \\ v \\ 1 \end{bmatrix} = \mathbf{A}\cdot[\mathbf{R}\,|\,\mathbf{t}]\cdot\begin{bmatrix} x_w \\ y_w \\ 0 \\ 1 \end{bmatrix} = \mathbf{A}\cdot[\mathbf{R}_{z=0}\,|\,\mathbf{t}]\begin{bmatrix} x_w \\ y_w \\ 1 \end{bmatrix} \tag{3}$$

where $R_{z=0}$ is equal to matrix **R** in which the third column has been deleted. Because of this, one point in the coordinate system of the 3D space and its image are related by means of a homography **H**, where

$$\mathbf{H} = \mathbf{A}\cdot[\mathbf{R}_{z=0}\,|\,\mathbf{t}] \tag{4}$$

3. DISTORTION MODELING

The pinhole camera does not include any kind of parameter relative to the distortions caused by the lens system. The most significant form of distortion is radial, which causes a shift in the radial direction of the point on the image respect to the principal point coordinates. This shift gives rise to two kinds of distortions on the radial direction, whether it occurs inwards (barrel distortion) or outwards (pincushion distortion). Such form of distortion can be modeled as an infinite series, as in

$$r_d = rf_{(r)} = r(1 + k_1 r^2 + k_2 r^4 + \ldots) \tag{5}$$

where r represents the distance from the principal point to the point on the image plane without distortion (the ideal), and r_d is the distance from the principal point to the observed (distorted) point with $r=(x^2+y^2)^{1/2}$, and k_i are the distortion coefficients. Nevertheless, it has been noticed (Tsai, 1987) that the inclusion of terms higher than k_2 contribute to improving the result but can produce numeric instability.. From (1) follows that

$$\begin{aligned} x_d &= xf_{(r)} = x(1 + k_1 r^2 + k_2 r^4 + \ldots) \\ y_d &= yf_{(r)} = y(1 + k_1 r^2 + k_2 r^4 + \ldots) \end{aligned} \tag{6}$$

where, by using expressions (1) and (2), it is easy to verify that

$$\begin{aligned} u_d &= u_0 + (u - u_0)(1 + k_1 r^2 + k_2 r^4 + \ldots) \\ v_d &= v_0 + (v - v_0)(1 + k_1 r^2 + k_2 r^4 + \ldots) \end{aligned} \tag{7}$$

It is worth mentioning that with the inclusion of terms higher than a k_1 there is no solution to (7) in a closed manner. The solution, then, must be reached through iterative methods.

4. PARAMETER ESTIMATION

4.1 Considerations upon the initial parameter estimate.

Many of the present methods for camera calibration make an initial estimate (in a closed form) of the set of parameters in order to use it as a starting point for a later, non-linear optimization stage as can be achieved by the Levenberg-Marquardt method (Press, *et al.*, 1992), which implies a great computational demand. The effect of distortions is not taken into consideration in the initial parameter estimate. In this work, we propose to consider the effect of the pinhole model deflections in the initial stage. For this reason, and assuming that the radial distortion is the predominant form in said deflections, we can make an estimate of the parameters in the region of the image where image distortions are relatively small: in the neighborhood of the principal point. But, in general, the principal point does not coincide with the center of the image, so in the first stage we must make an estimate of said point.

4.2 Estimation of the principal point.

In the calibration procedures based on planes, chessboard-like patterns are generally used. This is mainly due to the ease of detection of the control

points and to the ease of obtaining an accurate detection at sub-pixel level, as can be done through the method proposed in Harris and Stephens (Harris and Stephens, 1988). Let us make this our case. On such a pattern, we will consider each point on the line determining its position -in rows and columns- as if it were a matrix. Once the control points are detected on the image, what we obtain is a grid of points affected by the distortion of the lens system. This distortion, when considered in its radial form, has the principal point as its center. An indicator of the distortion degree is the deflection accumulated on the control points respect to the middle line to which they belong. If we consider a (model) plane "reasonably" parallel to the image plane, said accumulated deflections determine a distortion profile whose minimum corresponds to the principal point. This deflection is given by

$$D = \sum_{i=1}^{N} d_i \tag{8}$$

where d_1 represents the distance between the straight line $y = p_1 x + p_2$ and the point considered, and N is the number of points on the line considered. Parameters p_1 and p_2, which minimize the least mean squared error respect said straight line can be found as in Zhang, (Zhang, 1997) and they result from

$$\mathbf{p} = \begin{bmatrix} p_1 & p_2 \end{bmatrix} = (\mathbf{X}^T \cdot \mathbf{X})^{-1} \cdot \mathbf{X}^T \cdot \mathbf{Y} \tag{9}$$

with

$$\mathbf{X} = \begin{bmatrix} u_{d1} & u_{d2} & \cdots & u_{dN} \\ 1 & 1 & \cdots & 1 \end{bmatrix}^T, \mathbf{Y} = \begin{bmatrix} v_{d1} & v_{d2} & \cdots & v_{dN} \end{bmatrix}^T \tag{10}$$

where (u_{di}, v_{di}) are the coordinates -in pixels- of the control points on the image. So, once the accumulated deflections have been obtained by rows and columns on the model's grid, it is possible to estimate the principal point by means of the minimum of such deflections.

4.3 Estimation of a homography between the model's plane and the image.

From (3) and (4) we get that

$$\begin{cases} u = \dfrac{h_{11}x_w + h_{12}y_w + h_{13}}{h_{31}x_w + h_{32}y_w + h_{33}} \\ v = \dfrac{h_{21}x_w + h_{22}y_w + h_{23}}{h_{31}x_w + h_{32}y_w + h_{33}} \end{cases} \tag{11}$$

where h_{ij} represent elements of **H**. In this way,

$$\begin{bmatrix} x_w & y_w & 1 & 0 & 0 & 0 & -ux_w & -uy_w & -u \\ 0 & 0 & 0 & x_w & y_w & 1 & -vx_w & -vy_w & -v \end{bmatrix} \cdot \mathbf{h} = \mathbf{0} \tag{12}$$

with

$$\mathbf{h} = \begin{bmatrix} h_{11} & h_{12} & h_{13} & h_{21} & h_{22} & h_{23} & h_{31} & h_{32} & h_{33} \end{bmatrix}^T \tag{13}$$

With n control points whose images are within the neighborhood of the principal point estimated in section 2.2, n equations result as in (12), which together form a 2n x 9 matrix in the following way:

$$\mathbf{C}.\mathbf{h} = \mathbf{0} \tag{14}$$

The solution in (14) corresponds to the right singular-value associated to the least singular-vector of **C** and can be found by means of its singular value decomposition (SVD).

In order to contribute to the robustness of the general schema, it is necessary to proceed to a previous normalization as that described in Hartley (Hartley, 1995). In our case, an isotropic normalization proved to be good enough.

4.4 Estimation of the distortion coefficients

Unlike the complete set of intrinsic parameters (2), we will pose the problem for a reduced form as in

$$\mathbf{A} = \begin{bmatrix} f & 0 & u_0 \\ 0 & f & v_0 \\ 0 & 0 & 1 \end{bmatrix} \tag{15}$$

This results from considering the squareness of pixels (α=β=f) and orthogonal axes (c=0). Let us consider now a similar simplified form of the distortion model (5), including only up to the term which involves the k_1 coefficient. In this way, the result is

$$\begin{aligned} u_d &= u_0 + (u - u_0)(1 + k_1 r^2) \\ v_d &= v_0 + (v - v_0)(1 + k_1 r^2) \end{aligned} \tag{16}$$

with r^2=x^2+y^2. Now, by taking into account the reduced form (15), we have

$$u = fx + u_0, \qquad v = fy + v_0 \tag{17}$$

and so we can express (16) as

$$\begin{aligned} u_d &= u_0 + (u - u_0)(1 + k_1' r'^2) \\ v_d &= v_0 + (v - v_0)(1 + k_1' r'^2) \end{aligned} \tag{18}$$

where $k_1' = k_1 f^{-1}$, $r'^2 = (u - u_0)^2 + (v - v_0)^2$. Here, *(u, v)* are obtained on the basis of (11) and *(u_0, v_0)* are the coordinates of the principal point estimated in section (4.2) Then, we can express (18) as

$$\begin{bmatrix} (u - u_d) & (u - u_0) r'^2 \\ (v - v_d) & (v - v_0) r'^2 \end{bmatrix} \cdot \begin{bmatrix} 1 \\ k'_1 \end{bmatrix} = \mathbf{0} \tag{19}$$

By considering N points (the complete set of the model points), we can group them to form a 2N x 2 matrix. This matrix can be resolved in the same way as in (14). Once k_1' has been obtained, it is possible to solve (18) for *(u,v)* so as to improve the estimation of **H** by means of the solution in (14). This iterative procedure finishes when the value of k_1' becomes close enough to zero. It is worth mentioning that the

final value k_1' results from the addition of the values obtained in each iteration. This can be seen if we consider the following: let us call the value of k_1' - estimated in the iteration *i*- $k_{1(i)}'$; in this way,

$$\begin{aligned} r_{d(i)}' &= r_{(i)}'(1+k_{1(i)}'r_{(i)}'^2), \quad i=1,2,...,n \\ r_{(i)}' &= r_{d(i-1)}' \end{aligned} \tag{20}$$

here, under the observation that in real cameras $k_1' = k_1 f^{-1} \ll 1$, the above expression for $r_{d(i)}'$ can be approximated as $r_{(i)}'^2(1+2k_{1(i)}'r_{(i)}'^2)$. Then, solving (20) for the set of the $k_{1(i)}'$ obtained,

$$r_{d(n)}' = r_{(1)}'\left[1+\left(\sum_{j=1}^{n} k_{1(j)}'\right) r_{(1)}'^2\right] + K \tag{21}$$

where the first term of (21) includes the addition of the $k_{1(i)}'$ estimated, while term *K* includes products of the $k_{1(i)}'$ and powers of $r_{(n)}'$. Here, $\left|r_{(n)}'\right| \le M$, where *M* results from the size of the image, and the $k_{1(i)}'$ form a monotonous series with $\left|k_{1(i)}'\right| \to 0$. By considering the orders of magnitude of the factors, it can be seen that $K \to 0$.

4.5 Closed form solution to the camera calibration problem.

Following the method proposed by Zhang, two restrictions on the intrinsic parameters derived from the orthonormality of **R** are obtained, and hence, from (4):

$$\begin{aligned} \mathbf{h}_1^{cT}\left(\mathbf{A}^{-1}\right)^T \mathbf{A}^{-1}\mathbf{h}_2^c &= 0 \\ \mathbf{h}_1^{cT}\left(\mathbf{A}^{-1}\right)^T \mathbf{A}^{-1}\mathbf{h}_1^c - \mathbf{h}_2^{cT}\left(\mathbf{A}^{-1}\right)^T \mathbf{A}^{-1}\mathbf{h}_2^c &= 0 \end{aligned} \tag{22}$$

where $\mathbf{h}_i^c$ corresponds to the *i-th* column vector **H** – defined up to a scale factor, λ–. By considering

$$\mathbf{B} = \left(\mathbf{A}^{-1}\right)^T \mathbf{A}^{-1} \tag{23}$$

we can represent the symmetric matrix **B** (with $B_{12}=B_{21}=0$ and $B_{22}=B_{11}$) by means of vector

$$\mathbf{b} = \begin{bmatrix} B_{11} & B_{13} & B_{23} & B_{33} \end{bmatrix}^T \tag{24}$$

for which, based on (22), we have

$$\begin{bmatrix} h_{11}h_{12}+h_{21}h_{22} & h_{31}h_{12}+h_{11}h_{32} \\ h_{11}^2+h_{21}^2-h_{12}^2-h_{22}^2 & 2\left(h_{31}h_{11}-h_{12}h_{32}\right) \\ h_{31}h_{22}+h_{21}h_{32} & h_{31}h_{32} \\ 2\left(h_{31}h_{21}-h_{22}h_{32}\right) & h_{31}^2-h_{32}^2 \end{bmatrix} \mathbf{b} = \mathbf{0} \tag{25}$$

where h_{ij} represents elements of the **H** estimated homography. With the p ($p \ge 2$) images we can group the equations (25) corresponding to each image and form a 2p x 4 matrix **V**, thus resolving the system

$$\mathbf{V}\cdot\mathbf{b} = \mathbf{0} \tag{26}$$

whose solution is found in the same way as in (14). Considering that $\mathbf{B} = \lambda\left(\mathbf{A}^{-1}\right)^T \mathbf{A}^{-1}$, the intrinsic set of parameters results in

$$u_0 = -\frac{B_{13}}{B_{11}},\ v_0 = -\frac{B_{23}}{B_{11}},\ f = \sqrt{\frac{\lambda}{B_{11}}} \tag{27}$$

with $\lambda = B_{11}\left(B_{11}B_{33} - B_{13}^2 - B_{23}^2\right)$. Once matrix A has been obtained, the extrinsic set of parameters result from

$$\begin{aligned} \mathbf{r}_1^c &= \lambda\mathbf{A}^{-1}\mathbf{h}_1^c \quad \mathbf{r}_2^c = \lambda\mathbf{A}^{-1}\mathbf{h}_2^c \\ \mathbf{r}_3^c &= \mathbf{r}_1^c \times \mathbf{r}_2^c \quad \mathbf{t} = \lambda\mathbf{A}^{-1}\mathbf{h}_3^c \end{aligned} \tag{28}$$

where $\mathbf{r}_i^c$ represents the *i-th* column vector of **R** and $\lambda = 1/\left|\mathbf{A}^{-1}\mathbf{h}_1^c\right| = 1/\left|\mathbf{A}^{-1}\mathbf{h}_2^c\right|$. Due to the presence of noise, the estimated **R** matrix does not satisfy, in general, the properties of a rotation matrix. In Zhang (Zhang, 1998), a method is described for the estimation of a rotation matrix, **R'**, which may come close to **R** and which may minimize the Frobenius norm of the (**R'** – **R**) difference. The latter comes from **R'** = $\mathbf{UV}^T$, with **U** and **V** being the matrixes resulting from the singular value decomposition of **R**, in the equation: **R** = $\mathbf{USV}^T$.

4. EXPERIMENTAL RESULTS

The results reported by Zhang (Zhang, 1999), (method 1) were compared to those obtained with the method herein proposed (method 2) for the same set of images, which can be found in (Zhang, 1998). The data is shown in Table 1.

A comparison has been made between the results reported by Zhang, (method 1) and those obtained by using the method proposed, i.e. method 2. The same set of images adopted by Zhang (Zhang, 1998) was used in our case. Results are shown in Table 1.

Table 1. Results in the estimation of the principal point

	u_0	v_0
Reported by Zhang for five images	303.96	206.56
Image 1	289.95	217.07
Image 2	293.69	212.31
Image 3	281.24	216.69
Image 4	297.57	210.30
Image 5	293.14	203.57
Mean Value	291.12	211.99
Standard Deviation	6.15	5.52

In Fig. 1a -pixel coordinates- the following data is shown by way of example for image Nº 3: 1) geometrical centre of the image; 2) principal point resulting from using Zhang's method after

optimisation, and 3) principal point estimated by the procedure described in section 2.2.

In Fig. 1b the deflection profile obtained respect to the horizontal lines (left) and vertical lines (right) on the model's image is illustrated.

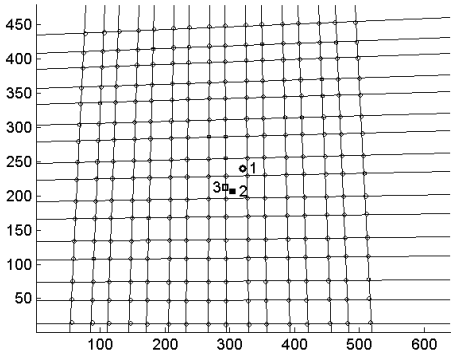

(a)

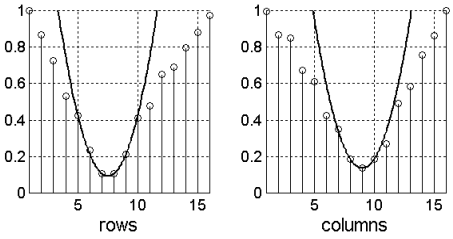

(b)

Fig. 1. (a) Estimation of the principal point, (b) accumulated dispersion respect to the mean lines.

In the estimation of the principal point, instead of adopting the minimum of the accumulated dispersions, the minimum of the parabola which better approaches the set of points formed by said minimum and its two adjacent points was considered. Better results are obtained by using a model with a greater quantity of points –a denser grid- so as to reduce the spacing between the lines. One way of achieving this is by means of an interpolation such as the one described in the paragraph above.

The results obtained with the procedure proposed as well as the comparison with those reported in Zhang (Zhang, 1999) are shown below. We adopted a radius of 150 pixels around the estimated principal point for the determination of the reduced homography between the model's plane and the image.

In the estimation of k_1, the number of iterations was limited to 10 for each image and, as a final value, the mean value was taken. Table 2 shows the results obtained for a variable number of images.

Table 2 Results obtained for 2, 3, 4 and 5 images

2 images			
parameter	method 1 Initial	Final	method 2
1: α/β, 2: f	825.59/ 825.26	830.47/ 830.24	837.20
u_0	295.79	307.06	300.45
v_0	217.79	206.55	207.03
k_1	0.161	-0.227	-0.202
k_2	-1.955	0.194	-
3 images			
parameter	method 1 Initial	Final	method 2
1: α/β, 2: f	917.65/ 920.53	830.80/ 830.69	833.11
u_0	277.09	305.77	300.72
v_0	223.36	206.42	206.15
k_1	0.128	-0.229	-0.205
k_2	-1.986	0.196	-
4 images			
parameter	method 1 Initial	Final	method 2
1: α/β, 2: f	876.62/ 876.22	831.81/ 831.82	831.07
u_0	301.31	304.53	301.77
v_0	220.06	206.79	206.85
k_1	0.145	-0.229	-0.205
k_2	-2.089	0.195	-
5 images			
parameter	method 1 Initial	Final	method 2
1: α/β, 2: f	877.16/ 876.80	832.50/ 832.53	832.80
u_0	301.04	303.96	301.08
v_0	220.41	206.56	207.01
k_1	0.136	-0.228	-0.206
k_2	-2.042	0.190	-

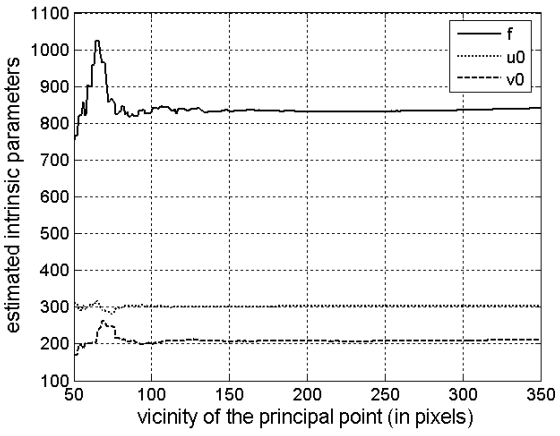

(a)

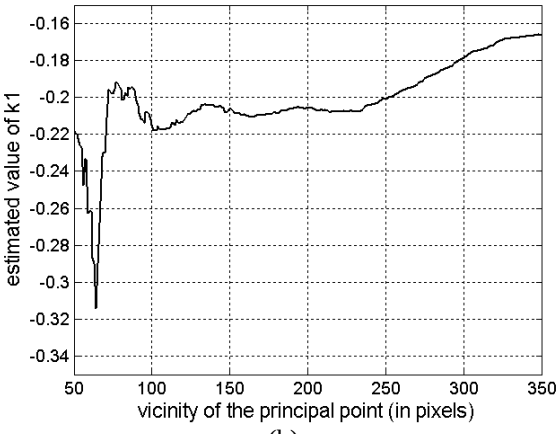

(b)

Figure 2. Variation of: (a) estimated intrinsic parameters and (b) distortion coefficient in terms of the neighbourhood of the (estimated) principal point considered.

In the results above, a remarkable improvement respect to the solution in the closed form proposed in Zhang (Zhang, 1999) can be seen, so much so that said results are very close to those obtained after an optimisation process.

Another noticeable advantage is that, as the quantity of images increases, the estimation on the parameters improves, and their values show a tendency to become very stable.

Still another difference occurs in the estimation of the distortion coefficients, and even though only the first one was considered, truly satisfactory results are achieved. In the case of Zhang's method, the estimation of said parameters in a closed form is very far from the final values obtained, and it is even an alternative choice to set them first to zero before proceeding to the final optimisation stage.

It is interesting to analyse the effect of the size of the neighbourhood around the principal point considered on the estimation of the parameters. Here follows an example for the case of 5 images (Fig. 2), and a variation of said neighbourhood from 50 to 350 pixels.

It can be seen that below a given value, the estimation made for different radii within a neighbourhood of the principal point is very erratic, but it becomes stable when said value is surpassed. This "threshold" value is, in the case under study, around 125 pixels. Above that value, the estimation on the intrinsic parameters becomes quite stable.

In the case of k_1, a progressive decay in the estimation is noticed as the radius of the neighbourhood considered increases. This impairment becomes more acute when a given value is surpassed, which, in our case, is around 250 pixels. The process takes place because, as we increase the radius of said neighbourhood, the effect of the lens distortion on the estimation of the homography between the model's plane and the image begins to increase too, and the estimation of the homography has a direct relation on the estimation of k_1'.

5. ACKNOWLEDGEMENTS

The authors feel deeply indebted to the members of the Centro de Investigación en Informática para la Ingeniería, CIII, (Research Centre for Engineering Informatics, RCEI) for their constant and unconditional support. This work was carried out at the National Technological University, Regional Faculty of Córdoba under grants from the National Agency for Promotion of Science and Technology (PICT03 Redes Nº 342 BID1201/OC-AR) and the National Technological University (UTN-25E070).

REFERENCES

Abdel-Aziz, Y. and H. Karara (1971). Direct linear transformation from comparator coordinates into object space coordinates. In: *close-range photogrammetry*, Papers from the American Society of Photogrammetry Symposium on Close-Range Photogrammetry, Urbana, Illinois 433, pp. 1-18.

Fusiello A., E. Trucco, and A. Verri (2000). A compact algorithm for rectification of stereo pairs, Machine Vision Applications., **vol. 12**, pp. 16-22.

Harris C. and M. Stephens (1988). A combined corner and edge detector, 4th ALVEY vision conference, pp 147--151.

Hartley R. I. (1994). An algorithm for self calibration from several views, Proc. Conference on Computer Vision and Pattern Recognition, Seattle, WA, pp 908-912.

Hartley R. (1995). In Defence of the 8-Point Algorithm, Proc. Fifth Int'l Conf. Computer Vision, pp. 1064-1070.

Heikkil J., & O. Silvn (1997). A Four-step Camera Calibration Procedure with Implicit Image Correction, IEEE Computer Society Conference on Computer Vision and Pattern Recognition, San Juan, Puerto Rico, pp. 1106-1112.

Knight J., A. Zisserman, I. Reid (2003),. Linear Auto-Calibration for Ground Plane Motion, Proc. Conference on Computer Vision and Pattern Recognition, pp 503-510.

Press W. H., S. Teukolsky, W. Vetterling, and B. Flannery (1992). *Numerical Recipes in C, Second Edition.* Cambridge University Press.

Farbiz F., S. Prince, A. D. Cheok, Wei Liu, ZhiYing Zhou, Ke Xu Ke, M. Billinghurst, H. Kato (2005). Live three-dimensional content for augmented reality. Multimedia, *IEEE Transactions on Multimedia* **Vol. 7**, Issue 3, pp 514-523.

Tsai R. Y. (1987), A versatile camera calibration technique for high-accuracy 3D machine vision metrology using off-the-shelf TV cameras and lenses. *IEEE Journal of Robotics and Automation*, 3(4):323-344.

Zhang Z. (1999), Flexible camera calibration by viewing a plane from unknown orientations. In Proc. of ICCV99, pp 666-673.

Zhang Z. (1997), Parameter estimation techniques: A tutorial with application to conic fitting, Image and Vision Computing, 15(1):59-76.

Zhang Z. (1998), A Flexible New Technique for Camera Calibration, Technical Report MSR-TR-98-71, Microsoft Research, http: // research.microsoft.com/ ~zhang/ calib/.